Supporting Information for:

Bio-inspired Fractal Textile Device for Rapid Sweat Collection and Monitoring

Yen-Chi Chen [a], Siang-Sin Shan [b], Yu-Te Liao[b] and Ying-Chih Liao[a]*

[a.] Department of Chemical Engineering, National Taiwan University, Taipei, Taiwan.

[b.] Department of Electrical and Computer Engineering, National Chiao Tung University, Hsinchu, Taiwan

* Corresponding author, E-mail: liaoy@ntu.edu.tw

Phone number: +886-2-3366-9688

Contents:

I. Sensor characterization.
II. Data processing example
III. Construction of fractal structure.
IV. Field test.

I. Sensor characterization and examples

There are two sensors in the device: a salt concentration sensor in the main flow channel and a sweat rate sensor in the reservoir sheet. The image of sensors is shown Figure S1(a). Both are screen printed electrodes using conductive carbon paste.

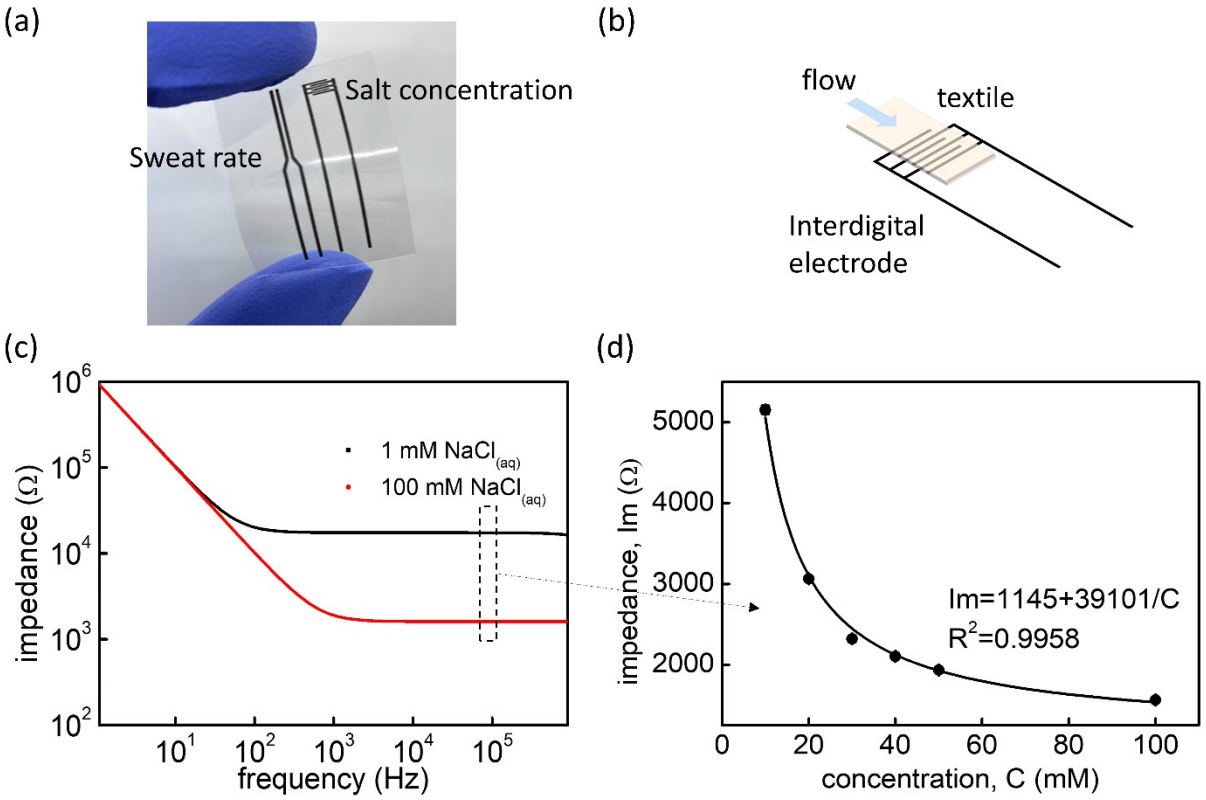

Figure S1. (a) Image of the sensors. (b) Schematic diagram of the salt concentration sensor. (c) EIS results of sample flow with concentration 1 mM and 100 mM. (d) Calibration curve of concentrations against measured impedance at 100 kHz.

A. Salt concentration

The salt concentration sensor is an interdigital electrode with 3 finger pairs (Figure S1(a)). The electrode is covered with a textile channel for continuous concentration monitoring. When sweat wicks from the collector to reservoir and wets the textile channel, the solution impedance between the interdigital electrode could be measured to determine the salt concentration of sweat.[1] To analyze solution resistance from impedance, an appropriate oscillation frequency needs to be determined. Electrochemical Impedance Spectroscopy (EIS) was done to characterize the sensor (Figure S1(c)). From the EIS results, 100 kHz is chosen for concentration/impedance conversion because of the plateau impedance for concentrations from 1 to 100 mM. A calibration curve was established by measuring the impedance of saline solutions with different concentration at frequency of 100 kHz. In the measurement, the sensor was covered by the textile channel and saline solutions with different concentration were wicked over the electrode to obtain impedance

values. A simple relationship[1] between concentration and the measured impedance can be obtained by regression as

$$Im = 1145 + 39101/C \quad (1)$$

where Im is the measured impedance and C is the concentration of the saline solutions. This equation will be used in the device for salt concentration determination.

B. Sweat rate sensor

The sensor is composed of two parallel lines printed with conductive carbon paste on a PET film (Figure S1(a)). The printed sensor is sandwiched between PET film and the textile-based reservoir (Figure S2(a)) to measure the water content and rate of change during wetting process. During the wetting process, the fluid is supplied from the center of the textile disk, fills the porous textile radially, and the radius of the wetted area increases gradually. The water absorption will result in significant change in the capacitance of the printed electrode (Figure S2(a)). Similar to those in section A, EIS is used to determine the appropriate frequency. From Figure S2(b), the impedance is irrelevant to concentration at lower frequency region (below 100 Hz), possibly because the capacitance component dominates at low frequency while the concentration-dependent resistance component is less important. In this frequency region, the impedance is dominated by the capacitance change, which is evidenced by the observed phase angle of 80^{o} (Figure S2(b)). Therefore, the change in capacitance at frequency 10 Hz is measured to infer the wetted area. To establish the relationship between water content and capacitance, saline (12.5 mM and 50 mM) is injected into the reservoir and corresponding capacitance is recorded as shown in Figure S2(c). With such calibration curve, the measured capacitance at any timestamp could be transformed into water content for sweat rate evaluation.

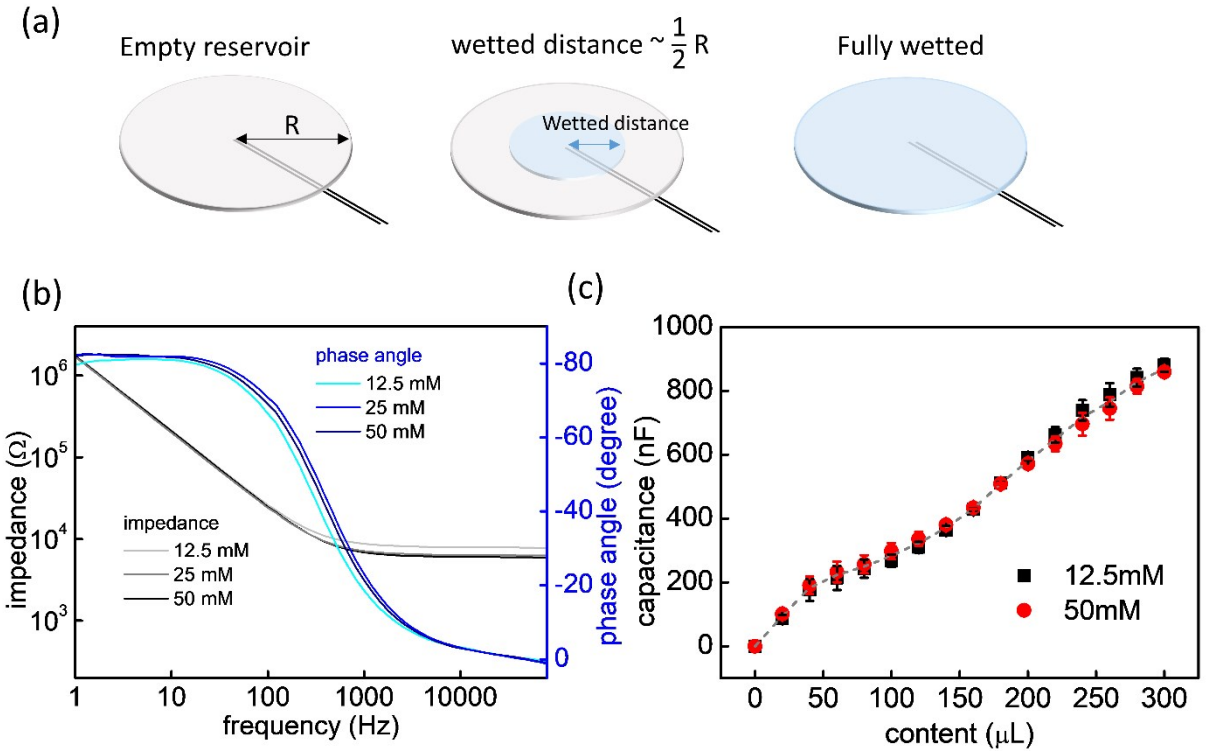

Figure S2. (a) Schematic diagram of the sweat rate sensor. (b) EIS of the electrode with same water content (75 μL) with different salt concentrations. (c) calibration curve: water content against capacitance (12.5 and 50 mM saline solution).

II. Data processing example

To test the accuracy of the sensors, the sweat collection device with a disk shape collector (Figure S3) is tested under a constant flux of 1 μL /cm^2/min. As shown in Figure S3(a), measurements from the concentration sensor, or impedance, can be transformed to concentration directly with equation (1). After conversion, the concentration at steady state is 50 mM, the same as the concentration of the injected saline solution. For sweat rate, the measured capacitance is first converted to water content by the interpolation on the curve established as S2(c). The weight measured from sweat rate sensor matches well with that from direct weighting measurements with an electronic balance, as shown in Figure S3(b). The content variation in a given time period (say 5 minutes) is divided by collection area (4.9 cm^2) for rate evaluation. The calculated flux is indicated by the grey labels.

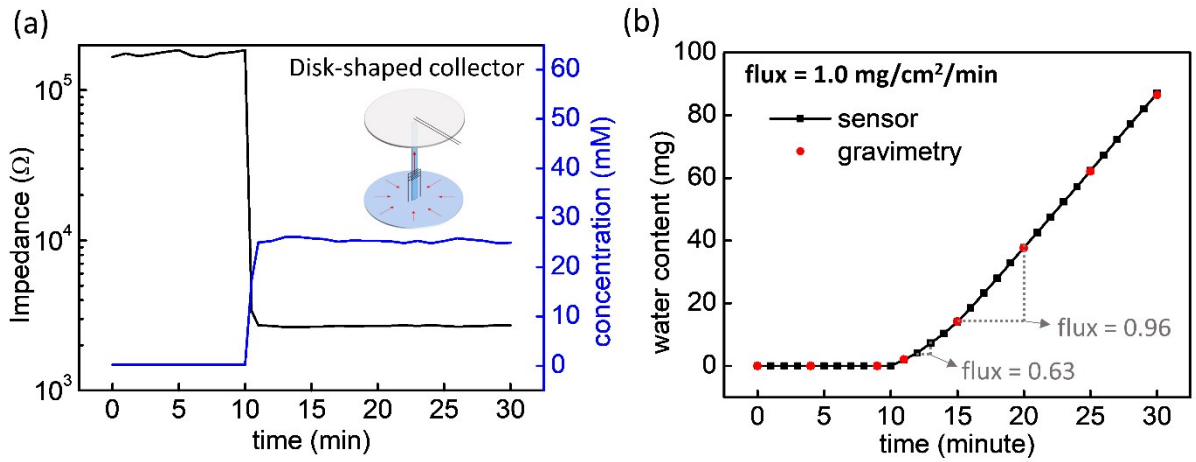

Figure S3. (a) Concentration measurement from the device with a disk-shape collector. (b) Water absorption test for the sweat rate sensor. The weight measured from sensor and electronic balance are compared. The sweat rate can be calculated from the area and slope of the weight curve.

III. Construction of fractal structure

A. Geometric structure and parameters

A fractal structure in a circular region is designed for rapid and effective sweat collection. The basic framework is based on the work by Wechsatol et al.[2] and is shown in Figure S4 (a). A basic framework within a circular region of radius *r* is shown in Figure S4(a). In the example of Figure 4, four mother branches bifurcate into eight (first generation) and sixteen (second generation) daughter branches with decreasing width. At each node, the branch is dichotomous instead of three or more bifurcations because dichotomous branches are advantageous over other designs in flow resistance and therefore are adopted here.[2] The first parameters in the structure is the number of mother branches in 0^{th} level, n, and the number of generations. These two parameters mostly determine the contour of the structure. Once the number of mother branches is selected, the 0^{th} bifurcation angle α can be calculated as

$$\alpha = 2\pi/n \qquad (2)$$

The value of α in the example of Figure 4 is 90^{o} or π/2.

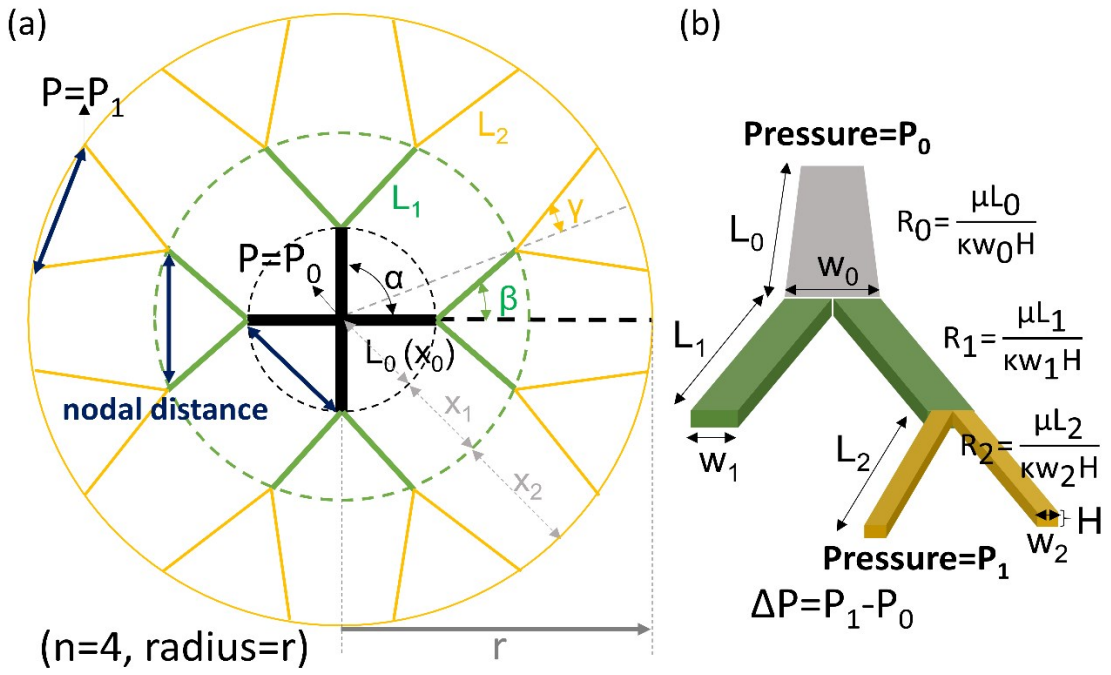

Figure S4. (a) Basic structure of fractal structure (n=4 and number of generations = 2) with indication of longest distance between nodes. (b) One of dichotomous main branch for width ratio derivation.

A fractal structure with only 2 generations (0^{th}, 1^{st}, and 2^{nd} generation) is adopted here to reduce the fabrication complexity. Although more generations could bring better access to sweat collection, the accompanied textile cutting and high flow resistance would be problemtic.[3] In our case, the branches after two bifurcations are delicate enough to contact the sub-millimeter scale sweat droplets within a circular region of 2.5 cm diameter. Other parameters include first and second bifurcation angle (β, γ), length of each generation (L_0, L_1, $L_{2...}$), and radius of concentric circles (x_0, x_0+x_1, $x_0+x_1+x_{2...}$). These terms could be expressed in the function of α and x_i as the following equations:

$$L_0 = x_0 \tag{3}$$

$$L_1 = \sqrt{\left[(x_0 + x_1)\left(\cos\frac{\alpha}{4}\right) - x_0\right]^2 + \left[(x_0 + x_1)\left(\sin\frac{\alpha}{4}\right)\right]^2} \tag{4}$$

$$L_2 = \sqrt{\left[(x_0 + x_1 + x_2)\left(\cos\frac{\alpha}{8}\right) - (x_0 + x_1)\right]^2 + \left[(x_0 + x_1 + x_2)\left(\sin\frac{\alpha}{8}\right)\right]^2} \tag{5}$$

$$\beta = \tan^{-1}\frac{(x_0 + x_1)\left(\sin\frac{\alpha}{4}\right)}{(x_0 + x_1)\left(\cos\frac{\alpha}{4}\right) - x_0} \tag{6}$$

$$\gamma = \tan^{-1} \frac{\left(x_0 + x_1 + x_2\right)\left(\sin\frac{\alpha}{8}\right)}{\left(x_0 + x_1 + x_2\right)\left(\cos\frac{\alpha}{8}\right) - \left(x_0 + x_1\right)} \tag{7}$$

$$x_0 + x_1 + x_2 = r \tag{8}$$

These relationships will be used in the next session of resistance modelling and geometry design optimization.

B. Optimal ratio of branching channel widths

Width of channel is crucial in the structure as it relates to the flow resistance. Low flow resistance is preferred for rapid removal of liquid. In the common applications, fractal structure is composed of hollow tubes. Hagen-Poiseuille equation is used to model the resistance of the laminar flow. A well-known ratio for radius ($r_1 = 2^{-1/3} r_0$) could be derived for resistance minimization with Lagrange multiplier.[4] Similar derivation could be done here by replacing the Hagen-Poiseuille equation with Darcy's law.

During the collection, sweat would move from the peripheral to the center due to capillary action. The collector is expected to distribute sparsely in the region to access sweat and transport with short delay. Besides, the gross volume of channels should be as low as possible to reduce induction or lag time. The flow rate of liquid, q, inside the channels is governed by Darcy's law:

$$q = \frac{\kappa A}{\mu L}\Delta P \tag{9}$$

where κ is the permeability of the porous media, μ is the viscosity of the liquid, L is the length of the channel, A is the cross-sectional area, and ΔP is the capillary pressure at liquid front, mostly related to the properties of medium. The term $\frac{\mu L}{\kappa A}\left(\frac{\Delta P}{q}\right)$ could also be viewed as the resistance of the channel, R. Considering a simple dichotomous case (Figure S4(b)), equation (9) could be expressed as

$$\Delta P = \frac{\mu L_0}{\kappa w_0 H} q + \frac{\mu L_1\, q}{\kappa w_1 H 2} + \frac{\mu L_2\, q}{\kappa w_2 H 4} = q\left(\frac{\mu L_0}{\kappa w_0 H} + \frac{\mu L_1}{2\kappa w_1 H} + \frac{\mu L_2}{4\kappa w_2 H}\right) = q\, R_{total} \tag{10}$$

where

$$R_{total} = \frac{\mu L_0}{\kappa w_0 H} + \frac{\mu L_1}{2\kappa w_1 H} + \frac{\mu L_2}{4\,\kappa w_2 H} \tag{11}$$

where H is the thickness of the textile channels.

The width ratio (w_1/w_0) can be optimized by finding the minimal transport resistance R_{total}. The structure is subject to a constraint of fixed total channel volume (V)

$$V = \left(L_0 w_o + 2 L_1 w_1 + 4 L_2 w_2\right) H \tag{12}$$

By multiplying the volume constraint with a Lagrange multiplier λ and added to the total resistance, one can obtain the objective function as:

$$R_{total}+\lambda V = \frac{\mu L_0}{\kappa w_0 H} + \frac{\mu L_1}{2\kappa w_1 H} + \frac{\mu L_2}{4\kappa w_2 H} + \lambda\left(L_0 w_o + 2 L_1 w_1 + 4 L_2 w_2\right) H \tag{13}$$

The partial differentiation of Eq. (13) with respect to w_0, w_1, w_2 are listed below and the optimal value occurs at all the differentiations become zero:

$$\frac{\partial R_{total}}{\partial w_0} + \lambda \frac{\partial V}{\partial w_0} = -\frac{\mu L_0}{\kappa w_0^2 H} + \lambda L_0 H = 0$$

$$\frac{\partial R_{total}}{\partial w_1} + \lambda \frac{\partial V}{\partial w_1} = -\frac{\mu L_1}{2\kappa w_1^2 H} + 2\lambda L_1 H = 0$$

$$\frac{\partial R_{total}}{\partial w_2} + \lambda \frac{\partial V}{\partial w_2} = -\frac{\mu L_2}{4\kappa w_2^2 H} + 4\lambda L_2 H = 0$$

The multiplier l can be solved individually as

$$\lambda = \frac{\mu}{\kappa H^2 w_0^2} = \frac{\mu}{4\kappa H^2 w_1^2} = \frac{\mu}{16\,\kappa H^2 w_2^2} \tag{14}$$

Thus, the result of optimal width ratio can be derived from simultaneous equations (14) as

$$w_0 = 2\, w_1 = 4\, w_2 \tag{15}$$

This width ratio relationship will be used in the fabrication of sweat collectors.

C. Distribution (spacing) of the channels

Besides the width ratios, length and bifurcation angles of the branching channels are also needed to determine fractal structures. In the literature[2, 5, 6], fractal structures for fluid transport are determined by minimizing the flow resistance from center to peripheral. Moreover, the uniformity of fluid absorption or temperature distribution can also be evaluated for optimal performance.[5, 6] In the case of sweat absorption, uniform contact to sweat or glands is the main issue. In the fractal structure, the branches diverge from the center to the nodes where they diverge again into next generation. Within any generations, the longest peripheral distance between channels would occur at the nodes as shown in Figure S4 (a). This nodal distance is the same as the arc dissected by the branches. For effective collection, the peripheral nodal distances are kept constant throughout the structure to cover the absorption area. In the case of two generations, the following relationship will hold:

$$\frac{2\pi x_0}{n} = \frac{2\pi(x_0 + x_1)}{2n} = \frac{2\pi(x_0 + x_1 + x_2)}{4n} \quad (16)$$

With this simplification, one can obtain the ratio of circular radii in each generation as

$$x_0 : x_1 : x_2 = 1 : 1 : 2 \quad (17)$$

Consequently, the dimensionless radii of concentric circles (x_0, x_1, x_2) are 0.25r, 0.25r, and 0.5r respectively. Using Eq. (17) and a given n, other parameters (β, γ, and L_i's) could be derived from equations (3) to (8). Such fractal structures are demonstrated in Figure S5(a) and the detailed parameters are listed in Table S2 with r =1. Images of fabricated fractal collector (n=6, 8, 10. r = 1.25 cm) and their coverage on a holey film are shown in Figure S5(b).

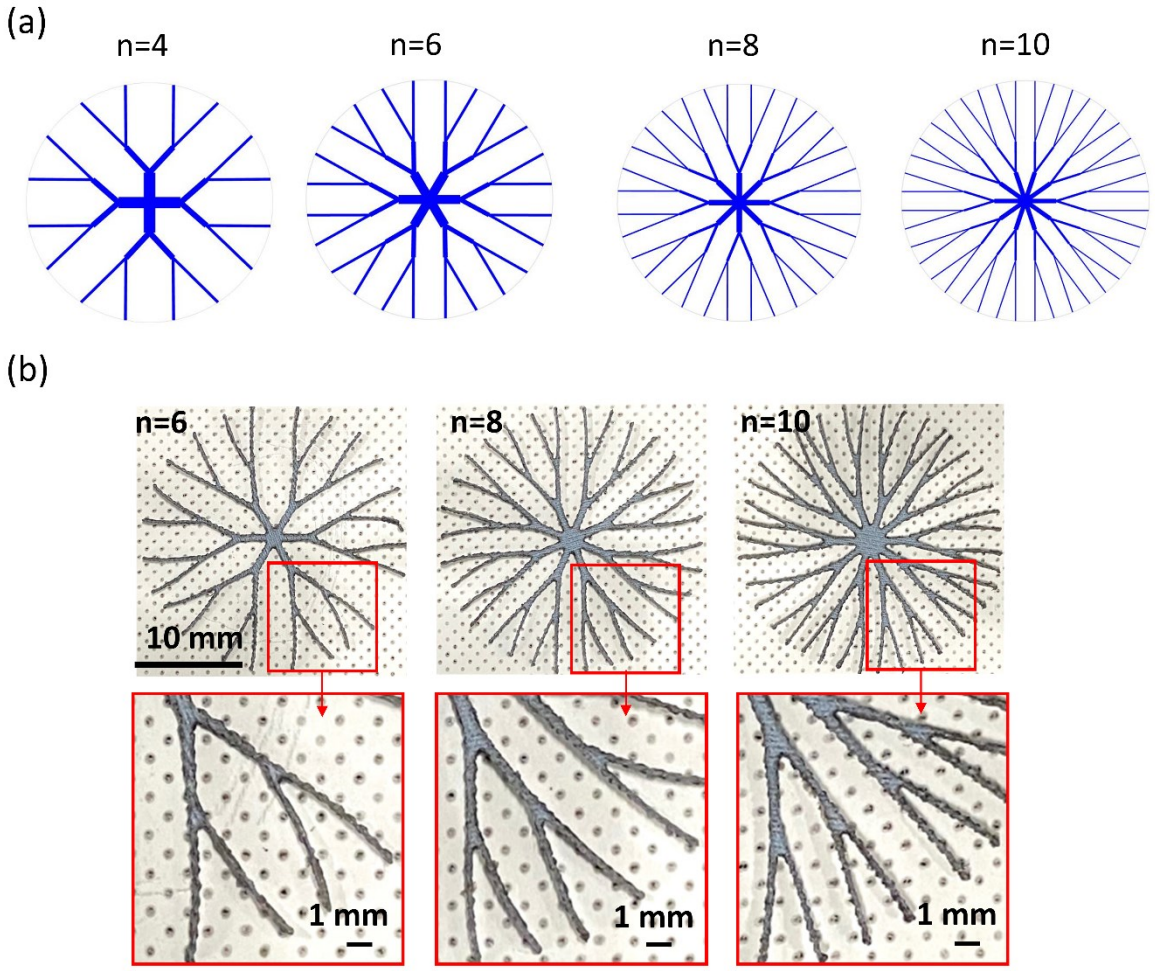

Figure S5. (a) Images of fractal structure designs with different main branches numbers n. A uniform nodal spacing method is used and marked with arrows. (b) Images of fabricated fractal collector (n=6, 8, 10) and the coverage on a holey film

Table S2. Calculated parameters for the optimal fractal structures.

n	α *	β *	γ *	L_0/r	L_1/r	L_2/r	f
3	2.094	0.939	0.507	0.25	0.310	0.533	1.194
4	1.571	0.734	0.385	0.25	0.286	0.519	1.112
5	1.257	0.601	0.310	0.25	0.273	0.512	1.072
6	1.047	0.507	0.260	0.25	0.266	0.508	1.051
7	0.898	0.438	0.223	0.25	0.262	0.506	1.037
8	0.785	0.385	0.195	0.25	0.259	0.505	1.029
9	0.698	0.344	0.174	0.25	0.257	0.504	1.023
10	0.628	0.310	0.157	0.25	0.256	0.503	1.018
11	0.571	0.283	0.142	0.25	0.255	0.503	1.015
12	0.524	0.260	0.131	0.25	0.254	0.502	1.013
13	0.483	0.240	0.121	0.25	0.254	0.502	1.011
14	0.449	0.223	0.112	0.25	0.253	0.502	1.009
15	0.419	0.208	0.105	0.25	0.253	0.501	1.008
16	0.393	0.195	0.098	0.25	0.252	0.501	1.007

* The unit of α, β, and γ are in rad.

D. Calculation Results

After the structure is determined, the collection effectiveness or flow resistance are calculated to evaluate the optimal performance. Herein, we investigate the impact of number of braches on flow resistance by summing up the contribution from all generations[2].

$$\Delta P = \Delta P_0 + \Delta P_1 + \Delta P_2 = \frac{q\,\mu}{n\kappa H}\left(\frac{L_0}{w_0} + \frac{L_1}{2w_1} + \frac{L_2}{4w_2}\right) \quad (18)$$

The pressure difference could be considered constant since it is only determined by capillary pressure at the liquid front. Another parameter we concern is the maximum wicking rate, q, which is limited by the flow resistance. For comparison, we assume that all channel volume (V_t) is constant similar to what we did in the previous section.

$$V_t = n \times V = n\,H(w_0L_0 + 2w_1L_1 + 4w_2L_2) \quad (19)$$

Combining equation (15), (18) and (19), one could get:

$$\Delta P/q = \frac{\mu}{\kappa V t}(L_0 + L_1 + L_2)^2 \quad (20)$$

The dimensionless flow resistance is

$$f \equiv (\kappa V t\, \Delta P)/(\mu q r2) = (L_0 + L_1 + L_2)^2/r^2 \quad (21)$$

In Eq. (21), n is eliminated and the total resistance is only a function of channel lengths due to the fixed total volume. In Figure S6, the calculation results show that the dimensionless total resistance f decreases to unity as n increases. The distribution of channels becomes crowded as n increases (Figure S5(a)), making total length of branches ($L_0 + L_1 + L_2$) close to the radius r. More branches are preferable for minimal resistance, but the effect of resistance reduction becomes trivial after n>8.

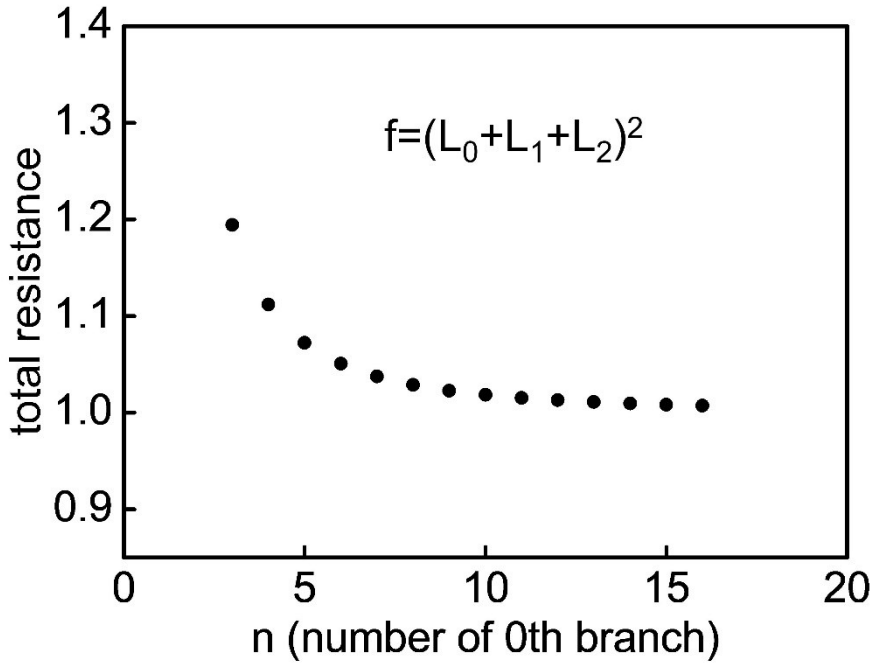

Figure S6. Relationship between n and total resistance in the fractal structure.

IV. Field test

To validate the capability of the device to work at highly sweating region, the device was worn on forehead for a test (Figure S7). During the test, the measured sweat rate increased quickly and peaked at roughly 3 μL /cm^2/min, suggesting the feasibility of the device to operate under high flux rate conditions.

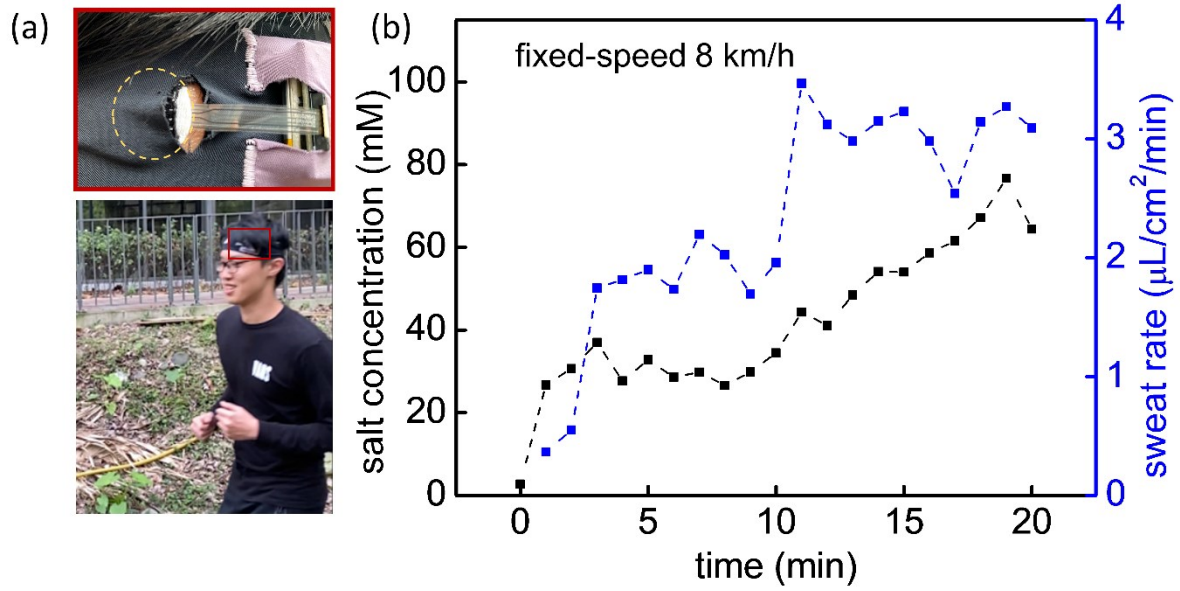

Figure S7. On-body continuous monitoring (a) device wore on forehead (b) salt concentration and sweat rate profile during a fixed-speed

References

1 M. Ibrahim, J. Claudel, D. Kourtiche, M. Nadi, Journal of Electrical Bioimpedance. 2013;**4**,13-22.

2 W. Wechsatol, S. Lorente, A. Bejan, International Journal of Heat and Mass Transfer. 2002;**45**,4911-24.

3 A. H. Reis, A. F. Miguel, M. Aydin, Medical Physics. 2004;**31**,1135-40.

4 A. Miguel, Journal of Applied Fluid Mechanics. 2019;**12**,1223-9.

5 X.-Q. Wang, A. S. Mujumdar, C. Yap, Journal of Applied Physics. 2007;**102**,073530.

6 X.-Q. Wang, P. Xu, A. S. Mujumdar, C. Yap, International Journal of Thermal Sciences. 2010;**49**,272-80.